An Efficient Algorithm for Locating TE and TM Poles for a Class of Multiscale Inhomogeneous Media Problems

Kalyan C. Durbhakula, *Student Member, IEEE*, Deb Chatterjee, *Senior Member, IEEE*, and Ahmed M. Hassan, *Senior Member, IEEE*

***Abstract*—The Mittag–Leffler (ML) expansion method has been minimally studied in the electromagnetic theory community. Therefore, in this article, the ML expansion functions are effectively utilized to locate initial poles for practical dielectric materials backed by a ground plane. The initial poles from the ML expansion and other existing methods are, then, checked for convergence, and found that the proposed method is highly efficient for electrically thick substrates (ETSs). To understand why, a fundamental and intrinsic convergence (in terms of relative or absolute errors) analysis of ML expansion and Taylor series expansion functions has been carried out and it was found out that the ML expansion converges significantly faster. In addition, Padè approximant has been successfully applied at no computational expense to improve the accuracy of initial pole locations. Moreover, proper and improper surface wave (SW) modes have been clearly distinguished from the poles obtained using the ML expansion method. Finally, the spectral region between leaky and SW poles for ETSs is identified using the initial pole locations obtained from using the ML expansion function on the transverse electric characteristic mode equation.**

***Index Terms*—Complex functions, Green's Functions (GF), integral representations, leaky-wave (LW) poles, Mittag-Leffler (ML) expansion method, root finding algorithms, Sommerfeld radiation condition, surface wave (SW) poles, w-transformation.**

I. Introduction

GREEN'S functions (GFs) are paramount in developing full-wave electromagnetic (EM) solutions for printed circuit antennas and boards [1]. Upon carefully enforcing the boundary conditions of a certain environment and, then, deriving the GFs in the space-time domain, this will typically introduce Sommerfeld integrals (SIs). These SIs comprises of transverse magnetic (TM) and transverse electric (TE) multivalued reflection terms or transcendental expressions, which contain surface wave (SW) and leaky-wave (LW) poles. In numerical evaluation of SIs, these poles can easily be avoided by contour deformation techniques. On the other hand, the saddle point method approximates the SIs in closed form. Since accurate asymptotic calculation of SIs are required, it is effected by accurate numerical calculation of SW and LW poles that are singularities of the integrand in the complex domain. The asymptotic evaluation approach is usually fast but the process of finding poles especially for electrically thick substrates (ETSs) remains challenging.

Some of the important applications, which require information of SW poles to evaluate electric fields, include phased array antennas, microstrip transmission lines, and ultrawide band antennas [2], [3]. On the other hand, some other applications such as LW antennas require the identification of few improper LW poles, which are fast rising in nature up to a certain distance from the source [4], [5].

ETS have long been at the center of attraction due to bandwidth limitations in conventional microstrip antennas, whose dielectric thickness is electrically thin ($d << \lambda$) compared to operating wavelength. One well-known approach to increase the bandwidth is by increasing the thickness (electrically or by stacking multiple dielectrics) of the dielectric substrate. However, this requires the accurate localization of the dominant plus higher-order TM and TE poles. Several experiments were performed and complex numerical models have been developed to determine the resonant frequencies and the input impedance of microstrip antenna with ETS [6]–[10]. Interesting applications have been discovered, which requires improved EM techniques [11]–[13].

The goal of this article is to introduce accurate and fast pole identification method that works for both electrically thin and thick substrates. This, then, will be further utilized to calculate SIs with and without pole contribution. Several studies have reported different numerical and analytical methods to locate real and complex poles and further differentiate between SW and LW poles [14]–[20]. The multiscale phenomena in this article corresponds to the ability of Mittag–Leffler (ML) expansion functions to locate initial pole locations accurately for both electrically thin and thick substrates. Requirement for new multiscale models has been greatly addressed in the past [21]–[23]. To the best of our knowledge, the ML expansion method has only been used once in the field of EM to represent exact image theory calculations for layered medium [24]. However, we have used the ML expansion functions for the first time to determine

Manuscript received September 4, 2019; revised November 26, 2019; accepted December 27, 2019. Date of publication January 15, 2020; date of current version January 29, 2020. This work was supported by the CSEE Department, School of Computing and Engineering, UMKC. This paper was presented in part at the IEEE Int. Symposium on Antennas and Propagation, Atlanta, GA, USA. *(Corresponding author: Deb Chatterjee.)*

The authors are with the Department of Computer Science and Electrical Engineering, University of Missouri-Kansas City, Kansas City, MO 64110 USA (e-mail: kalyandurbhakula@mail.umkc.edu; chatd@umkc.edu; hassanam@umkc.edu).

Digital Object Identifier 10.1109/JMMCT.2020.2965108

SW and LW poles from transcendental equations. Our recent conference publications briefly explains the location of TM SW poles using the ML expansion functions [25], [26].

In this article, Section II briefly introduces the TE and TM modes of grounded single dielectric layer topology [27]. Section III begins with obtaining initial TM_0 SW poles for some realistic printed circuit board (PCB) materials [28] followed by a study of initial roots converging to their final root. This section also draws a conclusion on the behavior of ML expansion functions with an increase in the number of expansion terms [29]. Furthermore, we utilized the Padé approximant on ML expansion functions as convergence acceleration method [30]–[34]. In addition, the spectral region is identified from the initial poles obtained using the ML expansion functions [35]–[39]. Section IV concludes the article, followed by selected references.

II. Overview of TE and TM Modes

In this section, we recall TM and TE characteristic mode equations of grounded single dielectric layer medium [27]. The TE mode equation for a grounded single dielectric layer is given as

$$D_{\text{TE}} = \kappa_0 - j\kappa_1 \cot(\kappa_1\, d) = 0 \tag{1}$$

where κ_0, and κ_1 are longitudinal wave-numbers in layer 0 (free space) and layer 1 (dielectric medium), respectively. Also, d is the dielectric thickness. The TM mode equation reads as follows:

$$D_{TM} = \kappa_0 + j\frac{\kappa_1}{\varepsilon_r} \tan(\kappa_1\, d) = 0 \tag{2}$$

where ε_r is the relative permittivity of dielectric medium. Proper radiation condition must be employed in order to obtain appropriate polynomial equations. The radiation condition for the $\kappa_{0,1}$ is given as

$$\kappa_{0,1} = \begin{cases} \sqrt{k_{0,1}^2 - \xi^2}; & \xi \le k_{0,1} \\ \mp j\sqrt{\xi^2 - k_{0,1}^2}; & \xi > k_{0,1} \end{cases} \tag{3}$$

where $k_{0,1} = \omega\sqrt{\mu_{0,1}\varepsilon_{0,1}}$ is the intrinsic wavenumber of layer 0 and layer 1, $\varepsilon_1 = \varepsilon_0\varepsilon_r$, $\mu_1 = \mu_0\mu_r$, and $\mu_r = 1$. The μ_0 and ε_0 are the free space permeability and permittivity, respectively. In addition, the $-$ sign and $+$ sign in front of the second condition in (3) must be chosen appropriately to identify poles in the top sheet or bottom sheet, respectively. Finally, ξ is the unknown pole location that needs to be identified.

In [17], pole locations were obtained graphically by plotting the transcendental equations on a two-dimensional (2-D) contour map. However, the accuracy of this method increases with increase in number of 2-D grid points at the expense of computational time. On the other hand, the ML expansion function works by transforming a transcendental equation to a polynomial equation. The trigonometric functions present in (1) and (2) are expanded by their respective ML expansion functions, which are given as

$$\cot(\upsilon) = \frac{1}{\upsilon} - \sum_{m=1}^{\infty} \frac{1}{m^2\pi^2} \frac{2\upsilon}{1 - \left(\frac{\upsilon}{m\pi}\right)^2} \tag{4}$$

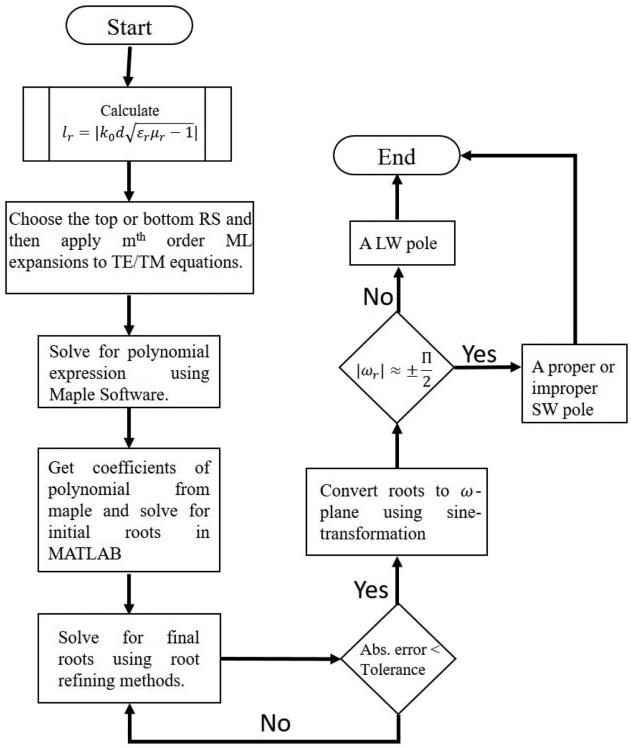

Fig. 1. Flowchart representation of obtaining SW and LW poles using the ML expansion functions.

and

$$\tan(\upsilon) = \sum_{m=0}^{\infty} \frac{8\upsilon}{[(2m+1)\pi]^2 - (2\upsilon)^2}. \tag{5}$$

In (4) and (5), υ is the expansion variable, and m is an integer. On using the substitutions $\upsilon = \kappa_1\, d$ and $u = \kappa_0\, d$ in (1) and (2) along with their corresponding ML expansion functions and radiation condition, one can obtain the required polynomial equation. For example, the polynomial equation to find TE SW poles in υ-plane is given by

$$\upsilon^6 + \upsilon^4(9 - l_r^2 - 2\pi^2) + \upsilon^2(\pi^4 - 2\pi^2 l_r^2 - 6\pi^2) + \pi^4(1 - l_r^2) = 0 \tag{6}$$

where $l_r = k_0 d\sqrt{\varepsilon_r - 1}$ and υ is the unknown pole location in υ-plane. The unknown pole location in ξ-plane is, then, obtained by back-substituting υ in $\kappa_1 = \upsilon/d$.

The polynomial equation shown in (6) is derived by substituting the first-order $\cot(\upsilon)$ ML expansion function, aforementioned υ, and u substitutions in (1) along with the radiation condition: $\kappa_0 = -j\sqrt{\xi^2 - k_0^2}$ and $\kappa_1 = \sqrt{k_1^2 - \xi^2}$. Other TE and TM polynomial equations can easily be derived and will be avoided in this article for brevity.

Fig. 1 shows a flowchart representation of the algorithm that has been employed to identify both types of poles for the TM and TE modes. The pole locations obtained from the ML expansion method are then compared against the pole approximation technique (PAT) [17] and the fast all modes (FAM) method [19]. One-to-one convergence comparison cannot be

TABLE I
ELECTRICAL PROPERTIES OF REALISTIC PCB MATERIALS

S.no	Product name	ε_r	$\tan\delta$ @ 10 GHz	d	$\lvert l_r\rvert$
1	Xtremespeed R01200 Laminates	3.05	0.0017	0.010"	0.0762
2	CLTE Series MW Laminates	3.10	0.0015	0.010"	0.0771
3	RT Duroid 5870	2.33	0.0012	0.062"	0.3806
4	RO 40360 G2	6.15	0.0038	0.032"	0.3866
5	AD 260A	2.60	0.0017	0.060"	0.4040
6	Kappa 438 Laminates	4.38	0.0050	0.060"	0.5872

TABLE II
DOMINANT TM_0 SW POLE—INITIAL ROOTS

$\lvert l_r\rvert$	ML expansion	PAT [17]	FAM [19]
0.0762	209.67 - $j1.4782\times10^{-4}$	205.12 - $j5.5518\times10^{-1}$	209.72 - $j2.2551\times10^{-4}$
0.0771	209.67 - $j1.2939\times10^{-4}$	207.54 - $j4.9208\times10^{-1}$	209.72 - $j1.9742\times10^{-4}$
0.3806	212.22 - $j5.3957\times10^{-3}$	213.64 - $j2.8743\times10^{-1}$	213.60 - $j8.4440\times10^{-3}$
0.3866	211.16 - $j3.2484\times10^{-3}$	213.97 - $j2.3988$	212.04 - $j5.4312\times10^{-3}$
0.4040	212.50 - $j7.2951\times10^{-3}$	214.49 - $j4.5259\times10^{-1}$	214.06 - $j1.1562\times10^{-2}$
0.5872	214.97 - $j2.6989\times10^{-2}$	218.08 - $j2.2055$	218.16 - $j4.7333\times10^{-2}$

derived between the ML expansion method and the PAT because the latter method is a graphical technique. On the other hand, the FAM method uses Taylor series (TS) expansion functions to replace the trigonometric functions. Therefore, a convergence comparison can be drawn between the ML and TS expansion functions and the details have been laid out in the results section.

The TS expansion functions for $\tan(\upsilon)$ and $\cot(\upsilon)$ are given as follows:

$$\cot(\upsilon) = \sum_{m=0}^{\infty} \frac{(-1)^m 2^{2\,m} B_{2\,m}}{(2\,m)!} \upsilon^{2m-1} \tag{7}$$

$$\tan(\upsilon) = \sum_{m=1}^{\infty} \frac{(-1)^{m-1} 2^{2\,m} (2^{2\,m}-1) B_{2\,m}}{(2\,m)!} \upsilon^{2m-1}. \tag{8}$$

In (7) and (8), $B_{2\,m}$ indicates Bernoulli numbers [29].

III. RESULTS AND DISCUSSION

Table I shows the electrical properties of some practical PCB materials, whose data are obtained from Rogers Corporation [28]. As one can notice from Table I, the value of $|l_r|$ calculated at 10 GHz is below $\pi/2$, which indicates that there is at least one dominant TM_0 SW pole and few TM and TE LW poles. With the demand for increase in operating frequency, the materials mentioned in Table I might start acting as ETS. Some of the physical LW modes at 10 GHz might transition into improper or proper SW modes as the frequency increases. We examine more of this transition behavior in Section III-F.

A. Convergence Between Root Finding Algorithms

In [25], a brief discussion on initial TE SW poles and their final pole locations was reported. The initial pole location for each substrate configuration was obtained by the ML expansion, PAT [17], and FAM [19] methods. The final pole location was, then, obtained by using the Newton–Raphson root-finding method. In this section, we expanded the scope and investigated the convergence factor "number of iterations to final root" between various root-finding algorithms. Besides Newton–Raphson method, Muller's and Regula-Falsi methods have been employed to draw the convergence comparison.

To test the convergence factor from each root-finding method, we calculated the dominant TM_0 SW pole for the materials shown in Table I from the ML expansion, PAT [17], and FAM [19] methods. The initial pole locations obtained from the ML expansion, PAT [17], and FAM [19] methods are compared against each other, which are shown in Table II. In the case of ML expansion and FAM methods, only the first-order expansion term was deemed sufficient. The PAT, being a graphical method, plots the entire transcendental equation on a 2-D contour graph [17]. The accuracy of PAT is determined by the number of 2-D mesh-grid points employed to plot the transcendental equations. In order to identify an accurate initial pole location using the PAT, large number of grid points must be employed, which further increases the computational time. However, the ML expansion and FAM methods are capable of identifying these locations by employing only the first-order expansion term.

The number of iterations taken by each root-finding algorithm to reach to a final root for different $|l_r|$ values is shown in Tables III and IV. The number of 2-D grid points used for PAT in Tables III and IV is 500 $\times$ 500. In Table III, the six rows calculates and compares number of iterations for six PCB materials shown in Table I, respectively. Table IV calculates and compares number of iterations at different operating frequencies for the Kappa 438 Laminates PCB material. From Tables III and IV, it can be concluded that the first-order ML expansion function has significant advantage over the other two methods in identifying the dominant TM_0 SW pole. In other words, one can notice that the number of iterations used by the ML expansion method to reach to the final root is consistent for most of the cases irrespective of the change in $|l_r|$. On the other hand, the accuracy of FAM decreases as the value of $|l_r|$ increases as shown in Table IV. ETS are generally identified with higher $|l_r|$ values, typically $|l_r| > \pi/2$. Recent developments in the antenna design using PCB materials mentioned in Table I have vast applications to 5 G and satellite (ka-band) communications whose frequencies range between 24 and 55 GHz. The ML expansion method is primarily helpful in obtaining poles for such ETS.

B. Convergence Between ML and TS Expansion Functions

One of the key aspects of the ML expansion functions is its behavior near the singularity points. In this section, a detailed study is carried out to understand why ML expansion functions exhibit good convergence behavior. This section highlights the

TABLE III
FINAL ROOTS OF TM_0 SW POLE AND NUMBER OF ITERATIONS TO FINAL ROOT FOR $|l_r| < \pi/2$

f	$\lvert l_r \rvert$	Final Root	Number of Iterations to Final Root								
			Newton-Raphson			Muller's			Regula Falsi		
			ML	PAT	FAM	ML	PAT	FAM	ML	PAT	FAM
10 GHz	0.0762	209.72 - $j2.2441\times10^{-4}$	6	17	5	7	16	5	8	26	5
10 GHz	0.0771	209.72 - $j1.9642\times10^{-4}$	5	12	3	7	11	5	8	18	5
10 GHz	0.3806	213.42 - $j7.6875\times10^{-3}$	5	7	4	5	7	5	7	8	5
10 GHz	0.3866	211.91 - $j4.5941\times10^{-3}$	5	12	4	5	12	5	7	16	6
10 GHz	0.4040	213.83 - $j1.03340\times10^{-2}$	5	8	4	5	8	5	7	11	5
10 GHz	0.5872	217.22 - $j3.5784\times10^{-2}$	5	8	5	5	8	4	6	10	5

TABLE IV
FINAL ROOTS OF TM_0 SW POLE AND NUMBER OF ITERATIONS TO FINAL ROOT FOR $|l_r| > \pi/2$

f	$\lvert l_r \rvert$	Final Root	Number of Iterations to Final Root								
			Newton-Raphson			Muller's			Regula Falsi		
			ML	PAT	FAM	ML	PAT	FAM	ML	PAT	FAM
40 GHz	1.5225	1060.3 - $j0.5936$	5	5	27	5	4	9	6	6	620
40 GHz	1.5464	1306.8 - $j3.6101$	5	5	22	5	5	9	6	6	42
40 GHz	1.6161	1107.8 - $j0.9429$	5	5	63	5	5	10	6	6	412
45 GHz	1.7396	1625.3 - $j4.6145$	5	6	11	5	6	11	6	7	$>$10000
30 GHz	1.7617	991.44 - $j3.1584$	5	5	21	5	5	11	6	6	5290
40 GHz	2.3849	1244.7 - $j3.9347$	5	5	1583	5	5	$>$10000	6	6	$>$10000

relative (when the argument is real) and absolute (when the argument is complex) error between the ML, TS expansions of $\tan(\upsilon)$ and $\cot(\upsilon)$ trigonometric functions, and their exact values. The exact values are calculated using MALTAB's in-built trigonometric functions. This test was carried out for both real and complex input arguments. The ML expansion functions for the $\cot(\upsilon)$ and $\tan(\upsilon)$ trigonometric functions were shown in (4) and (5), respectively. Similarly, the TS expansion functions for $\cot(\upsilon)$ and $\tan(\upsilon)$ trigonometric functions were given in (7) and (8).

Tables V–VIII illustrates the convergence (rel. or abs. error) comparison between the ML, TS expansion functions, and the exact values. First column in Tables V–VIII indicate the argument value (real or complex). Second column shows the exact value of trigonometric function. Third column indicates number of expansion terms from the ML and TS expansion functions, which have been varied to show the significance of each method converging to exact value. Fourth and fifth columns show the output from ML expansion and rel/abs.error (between the ML expansion value and the exact value), respectively. Similarly, sixth and seventh columns show the output from TS expansion and rel/abs.error (between the TS expansion value and the exact vale), respectively.

In Table V, the ML rel. error for small argument values yielded higher error values when compared to the TS rel. error. However, as the argument increases, i.e., as the $\tan(\upsilon)$ trigonometric function reaches its singularity point, i.e., at $\pi/2$, the ML expansion showed good convergence. This is primarily due to the inverse series expansion seen with the ML expansion as opposed to the TS expansion. For example, for $\upsilon = 1.2$ in Table V, we could

TABLE V
CONVERGENCE COMPARISON OF $\tan(\upsilon)$ WHEN υ IS REAL

υ	$\tan(\upsilon)$	No. of Terms	ML expansion	ML Rel. Error (%)	TS expansion	TS Rel. Error (%)
0.05	0.05	1	0.0406	18.925	0.05	0.0834
0.05	0.05	11	0.0491	1.834	0.05	0.001
0.98	1.491	1	1.3006	12.7678	0.98	34.2705
0.98	1.491	11	1.4729	1.2104	1.4909	0.0027
1.2	2.5722	1	2.3360	9.1814	1.2	53.3465
1.2	2.5722	11	2.5501	0.8592	2.5659	0.2430
1.48	10.9834	1	10.6859	2.7086	1.48	86.5251
1.48	10.9834	11	10.9561	0.2482	8.0998	26.2540

TABLE VI
CONVERGENCE COMPARISON OF $\tan(\upsilon)$ WHEN υ IS COMPLEX

υ	$\tan(\upsilon)$	No. of Terms	ML expansion	ML Abs. Error (%)	TS expansion	TS Abs. Error (%)
0.05+j0.02	0.05 + j0.02	1	0.0405 + j0.0163	18.9308	0.05 + j0.02	0.0967
0.05+j0.02	0.05 + j0.02	11	0.0491 + j0.0197	1.8397	0.05 + j0.02	$1.28\times\ 10^{-14}$
0.98+j0.1	1.444 + j0.3143	1	1.2541 + j0.2939	12.9422	0.98 + j0.1	34.5943
0.98+j0.1	1.444 + j0.3143	11	1.4262 + j0.3124	1.2273	1.4443 + j0.3143	0.003
1.2+j0.05	2.5241 + j0.3743	1	2.2879 + j0.3637	9.2625	1.2 + j0.05	53.4234
1.2+j0.05	2.5241 + j0.3743	11	2.5020 + j0.3734	0.8669	2.5210 + j0.3687	0.2476
1.48+j0.07	6.8776 + j5.3490	1	6.5802 + j5.3332	3.4177	1.48 + j0.07	86.6535
1.48+j0.07	6.8776 + j5.3490	11	6.8503 + j5.3477	0.3133	7.2278 + j3.0328	26.8859

TABLE VII
CONVERGENCE COMPARISON OF $\cot(\upsilon)$ WHEN υ IS REAL

υ	$\cot(\upsilon)$	No. of Terms	ML expansion	ML Rel. Error (%)	TS expansion	TS Rel. Error (%)
0.005	199.9983	1	199.9990	$3\times\ 10^{-4}$	200	8.3×10^{-4}
0.02	49.9933	1	49.9959	0.0052	50	0.0133
0.05	19.9833	1	19.9899	0.0327	20	0.0833
0.98	0.6707	1	0.8004	19.3379	1.0204	52.1386
0.98	0.6707	11	0.6880	2.5737	0.6707	$2.4\times\ 10^{-9}$
1.48	0.091	1	0.02902	218.7586	0.6757	642.1202

TABLE VIII
CONVERGENCE COMPARISON OF $\cot(\upsilon)$ WHEN υ IS COMPLEX

υ	$\cot(\upsilon)$	No. of Terms	ML expansion	ML Rel. Error (%)	TS expansion	TS Rel. Error (%)
0.005+j0.001	192.31 - j38.462	1	192.31 - j38.462	$3.3\times\ 10^{-4}$	192.31 - j38.462	8.6×10^{-4}
0.02+j0.01	39.9933 - j20.003	1	39.9959 - j20.002	0.0065	40 - j20	0.0167
0.05+j0.01	19.2141 - j3.8495	1	19.2206 - j3.8482	0.034	19.2308 - j3.8462	0.0867
0.98+j0.1	0.6611 - j0.1439	1	0.7907 - j0.1303	19.2674	1.0099 - j0.1301	51.9063
0.98+j0.1	0.6611 - j0.1439	11	0.6784 - j0.1421	2.5647	0.6611 - j0.1439	$2.7\times\ 10^{-9}$
1.48+j0.07	0.0906 - j0.0705	1	0.02897 - j0.0605	173.72	0.6742 - j0.0319	509.56

notice that by using only one expansion term, the output value from the ML expansion is much closer to the exact value than the output from the TS expansion. A similar observation can be made at $\upsilon = 1.48$ when number of expansion terms equal to 1. On the other hand, the rel. error from TS expansion deteriorated with increase in number of expansion functions from 1 term to 11 terms. This indicates that the TS expansion near the singularity points converges poorly.

Table VI shows the results for the complex argument. A similar behavior can be observed from the ML and TS expansion functions. The ML expansion functions behave well, especially near the singularity point. Both real and complex argument results from the first-order ML expansion function agrees reasonably well with the exact form. This result implies that the ML expansion method is capable of finding accurate initial complex poles, which are the LW poles.

Next, we investigate the behavior of $\cot(\upsilon)$ trigonometric function in Tables VII and VIII. A singularity for cotangent functions can be observed for multiples of $n\pi$, i.e., for $n = 0, 1, 2, \ldots$ and so on. In Table VII, for small argument values, good convergence is seen from both methods on using only the first-order expansion term. Even with the increase in υ, the rel. error from ML expansion is smaller than the rel. error from TS expansion. Table VIII also indicates similar observations. By employing the higher-order expansion terms, the rel. error from TS expansion improves. However, this increases the computational time in order to obtain the higher-order equations. This problem can be easily avoided by employing only the first-order ML expansion function for the trigonometric function present in the TE and TM mode equations.

C. Normalized Root-Mean-Square Error (NRMSE)

The NRMSE method has been utilized to compare the efficiency of ML, PAT, and FAM methods for different dielectric permittivities and thickness. The NRMSE is calculated as follows [40]:

$$\text{NRMSE} = \frac{\sqrt{\sum_{i=1}^{n} \frac{(x_{\text{initial}} - x_{\text{final}})^2}{n}}}{\text{mean}(x_{\text{final}})} \tag{9}$$

where x_{initial} is the initial root obtained from the ML, or PAT or FAM methods, x_{final} is the final root obtained after using Newton–Raphson root-finding algorithm, and n is the number of data points. In this case, the value of n is one since the error is calculated between each initial and final root for a particular value of permittivity or thickness. Alternatively, one can also calculate the NRMSE for a range of permittivity values at each dielectric thickness value, where the value of n is equal to the total number of permittivity values. The initial and final root values used to calculate the NRMSE in this section are the initial and final poles of dominant TM_0 SW mode. An NRMSE value close to zero can be interpreted as perfect fit. Fig. 2 shows the NRMSE calculated for a range of dielectric permittivity values (top) and for different dielectric thickness (bottom). From both results, it is clear that the NRMSE from ML expansion method is closer to zero than the other methods. Moreover, as the permittivity or thickness increases, the NRMSE value from ML expansion method is decreasing, meaning reaching zero whereas the other methods are increasing. This result further validates the robustness of proposed method.

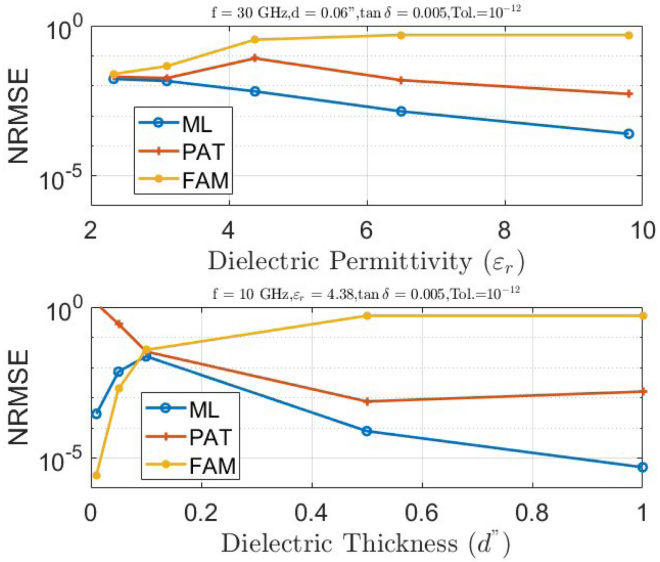

Fig. 2. Comparison of NRMSE between three methods for different dielectric permittivities (top) and dielectric thickness (bottom).

D. Padé Approximant

The Padé approximant has proved its usefulness in modeling and approximating the time delay output response of continuous time domain systems. This method is particularly useful when a power series diverges or converges slowly when using multiple expansion terms [31], [34]. On the other hand, the Padé approximant could diverge if the expansion point is close to a pole or zero.

In this section, we test the convergence limits of Padé approximant by applying them on polynomial equations of D_{TE} derived using the ML expansion functions. In general, a Padé approximant represents any power series in terms of rational functions, which is defined as follows [31]:

$$P_M^N(\upsilon) = \frac{N_j(\upsilon)}{D_j(\upsilon)} = \frac{\sum_{j=0}^{N} a_j \upsilon^j}{\sum_{j=0}^{M} b_j \upsilon^j}. \tag{10}$$

Now, consider $f(\upsilon)$ to be the polynomial equation of D_{TE} or D_{TM} obtained using the ML expansion functions

$$f(\upsilon) = \sum_{i=0}^{k} \lambda_i \upsilon^i \tag{11}$$

where $\lambda_0, \lambda_1, \ldots \lambda_k$ are the known coefficients of the polynomial equation. To maintain generality with most expansions, the first coefficient in denominator of (10) is set to 1, i.e., $b_0 = 1$. Therefore, we get $N + 1$ and M unknown coefficients in the numerator and denominator of (10), respectively. The unknown coefficients $a_0, a_1, \ldots, a_N$ and $b_1, b_2, \ldots, b_M$ are, then, determined by equating coefficients of similar powers from (10)

TABLE IX
PADÉ APPROXIMANT OF TE_1 SW POLE EVALUATED AT $|l_r|$=1.8850

m	Padé approximant $P_M^N(\upsilon)$	No. of iterations to final root
1	$P_3^3(\upsilon) = 226.1579$	5
2	$P_2^2(\upsilon) = P_3^2(\upsilon) = P_3^3(\upsilon) = 228.7036$	5
2	$P_3^4(\upsilon) = 211.5592$	6
2	$P_4^4(\upsilon) = P_4^5(\upsilon) = P_5^4(\upsilon) = P_5^5(\upsilon) = 211.9514$	6

and (11), which reads as

$$f(\upsilon) = \frac{N_j(\upsilon)}{D_j(\upsilon)}. \tag{12}$$

Let us recall the $\mathrm{D_{TE}}$ polynomial equation (6), which can be rewritten as follows:

$$f(\upsilon) = \lambda_6\upsilon^6 + \lambda_4\upsilon^4 + \lambda_2\upsilon^2 + \lambda_0\pi^4 \tag{13}$$

where

$$\begin{aligned}\lambda_0 &= \pi^4(1 - l_r^2)\\ \lambda_1 &= \lambda_3 = \lambda_5 = 0\\ \lambda_2 &= \pi^4 - 2\pi^2 l_r^2 - 6\pi^2\\ \lambda_4 &= 9 - l_r^2 - 2\pi^2\\ \lambda_6 &= 1.\end{aligned} \tag{14}$$

By using in-built Padé approximant functions available in MATLAB and MAPLE, one can obtain the unknown a, b coefficients. The order of N, M must satisfy the condition $N + M = J$, where J is the highest order of the polynomial equation obtained using the ML expansion functions. The zeros of (10) will yield the pole locations in υ-plane, which can be converted to ξ-plane using (16).

For $m = 1$ and $m = 2$ ML expansions and for $|l_r| = 1.8850$ (f = 10 GHz, $\varepsilon_r = 10$, $\tan\delta = 0$, $d = 0.1\lambda$), the initial TE_1 SW pole location determined from their polynomial equation is 210.5082 and 214.7159, respectively. For the same configuration, the final TE_1 SW pole location is at 223.9544. The Padé approximant is, then, applied to the polynomial equations derived from the ML expansion method.

Table IX shows initial roots obtained from using Padé approximant for $m = 1$ and $m = 2$ expansions, as well as the number of iterations taken by the Newton–Raphson method to reach to the final root. For $m = 1$, only $P_3^3(\upsilon)$ predicted the initial pole location with highest accuracy.

The approximant from $P_0^0(\upsilon)$ to $P_1^2(\upsilon)$ could not predict SW pole due to limitation on the number of expansion terms. The zeros obtained by $P_2^2(\upsilon)$ and $P_3^2(\upsilon)$ are similar to the case of $P_3^3(\upsilon)$. Similarly, for $m = 2$, the $P_2^2(\upsilon)$, $P_3^2(\upsilon)$, and $P_3^3(\upsilon)$ predicted the initial location with higher accuracy than $m = 1$ case. Therefore, an optimum M, N value needs to be identified for a given substrate configuration in order to improve the accuracy of initial pole location. Similarly, the location of complex poles can be significantly improved by using optimum N, M values. The same can be said for D_{TM} characteristic mode equation. The Padé approximant is useful especially when predicting dominant and higher-order SW and LW poles for ETS with high tolerance.

TABLE X
NUMBER OF PROPER AND IMPROPER SW POLES

N+1 proper and N improper SW poles	
$\mathrm{D_{TE}}$	$(2\mathrm{N}+1)\frac{\pi}{2} < \lvert l_r \rvert < (2\mathrm{N}+3)\frac{\pi}{2}$
$\mathrm{D_{TM}}$	$\mathrm{N}\pi < \lvert l_r \rvert < (\mathrm{N}+1)\pi$

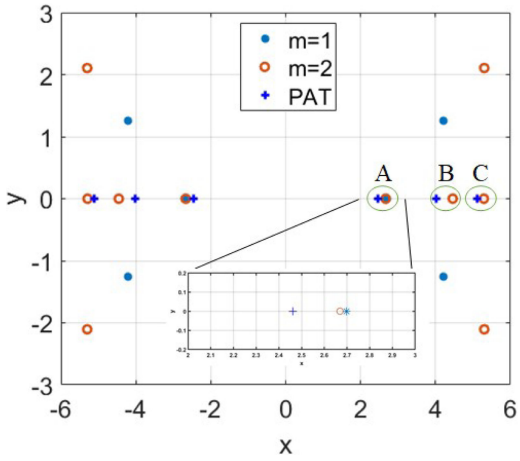

Fig. 3. SW and LW poles in the $\upsilon = x + jy$ domain.

E. Proper and Improper SW Poles

In the previous sections, much of the discussion was focused on obtaining initial pole locations using the first-order ML expansion function followed by convergence analysis. The focus in this section lies in showcasing that the ML expansion functions are capable of locating proper and improper SW poles accurately and quickly with a proper choice of expansion term—m in (4) and (5).

The first-order ML expansion could only identify dominant TM_0 SW and few TM, TE LW poles. However, in some cases, it was found that the first-order ML expansion function tends to miss improper SW poles, which arise as the value of $|l_r|$ increases.

Table X indicates the number of proper and improper SW poles that a dielectric substrate will generate depending on the value of $|l_r|$. In order to identify the improper SW poles, the value of m in (4) and (5) must be increased. For example, the first-order ML expansion in (4) enforcing on (1) returns a sixth-order polynomial equation, which produces six roots comprising of real and complex roots. The exact number of real and complex roots also depend on value of $|l_r|$. For $m = 2$, a tenth-order polynomial equation is obtained.

Fig. 3 shows real and complex pole locations of TE mode obtained from polynomial equations (derived using the ML expansion functions) for a particular substrate configuration (f = 1 GHz, $\varepsilon_r \approx 3.9$, $\tan\delta = 0$, $d = 0.5\lambda$) whose $|l_r| = 5.344$. For brevity, only $m = 1$ and $m = 2$ expansion terms have been

considered. The results from ML expansion method are, then, compared with the PAT [17]. The initial pole locations from the $m = 1$, $m = 2$ ML expansions, and the PAT are close to each other.

In Fig. 3, SW poles are located on the $y = 0$ line. From Table X, we can indicate that having $N = 1$ value satisfies the aforementioned $|l_r|$ value. Therefore, two proper SW poles and one improper SW pole are present and must be identified. Both positive and negative solutions in Fig. 3 will lead to unique solution, therefore we can consider any one side (i.e., positive side or negative side of x-axis) and investigate the differences between individual solutions on that particular side. Three SW poles can be noticed on the positive side of x-axis, which are grouped and labeled as A, B, and C.

The inset figure in Fig. 3 zooms in on the dominant SW pole generated by the $m = 1$, $m = 2$ expansion terms from the ML expansion functions and the dominant SW pole generated by the PAT [17]. In this inset figure, we can notice that the SW poles generated from the $m = 1$ and $m = 2$ ML expansion functions are very close to each other. However, the $m = 1$ ML expansion could predict only one SW pole (around $x = 2.7$ and $y = 0$), whereas, the $m = 2$ ML expansion predicted all three required SW poles. The three SW poles predicted by the $m = 2$ ML expansion agrees with the three SW poles predicted by the PAT [17].

To differentiate between proper and improper SW poles, sine transformation has been employed on the initial set of SW poles [35]

$$w = \sin^{-1}\left(\frac{\xi}{k_0}\right) \tag{15}$$

where

$$\xi = \sqrt{k_1^2 - \left(\frac{x + jy}{d}\right)^2}. \tag{16}$$

Once the initial w-estimates have been identified using (15), $\mathrm{D_{TE}}$ is evaluated with following κ_0 and κ_1 conditions:

$$\kappa_0 = -j\sqrt{\xi^2 - k_0^2} \tag{17}$$

$$\kappa_1 = +\sqrt{k_1^2 - \xi^2}. \tag{18}$$

The accurate w-value can be estimated using procedure described in [17]. Fig. 4 indicates the position of three SW poles obtained using the $m = 2$ ML expansion function in the w-plane.

In Fig. 4, poles A and C are identified as proper SW poles, whereas, pole B is an improper SW pole. Obviously, the LW poles always lie in the improper Riemann sheet, i.e., $w_r > 0$ and $w_i < 0$.

F. Spectral Region

The term spectral region was originally introduced by A. A. Oliner and since then it has been vastly used in the EM community to understand and generate SW and LW modes [38], [39].

Fig. 5 depicts a single dielectric layer geometry with complex permittivity and thickness (d) backed by a ground plane. The

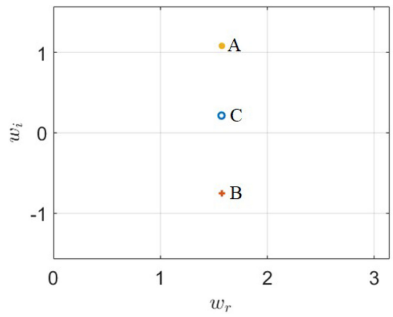

Fig. 4. SW poles in w-plane.

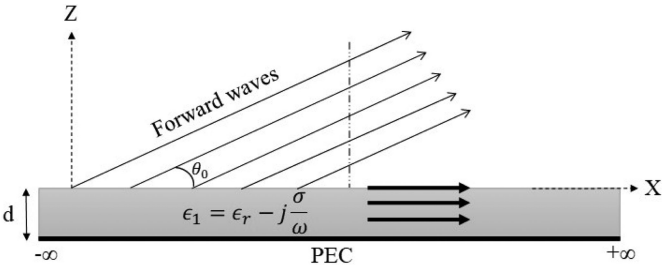

Fig. 5. Microstrip geometry indicating the guided modes and forward LW modes.

direction of a transmission line is along x-axis and the broadside is along z-axis. A line source existing inside the dielectric or on the dielectric–air interface generates certain SW and LW modes from the TM and TE mode equations. The guided modes, i.e., proper or improper SW modes in the transmission line direction are determined by [36]

$$k_x = \beta - j\alpha \tag{19}$$

where k_x is the longitudinal wavenumber, β is the phase constant, and α is the attenuation constant along the x-axis in Fig. 5. For a source present inside the dielectric, the complex wavenumber along the z-direction is given as

$$k_z = \pm(k_1^2 - k_x^2)^{1/2} \tag{20}$$

where $k_1 = k_{1r} - jk_{1i}$ and by considering $k_z = \beta_z - j\alpha_z$, we can establish a relation between modes in the horizontal and vertical direction. By squaring (20) on both sides and comparing only imaginary terms, we get

$$\alpha\beta - k_{1r}k_{1i} = -\alpha_z\beta_z. \tag{21}$$

From the above equation, if the dielectric substrate is lossless, (21) reduces to

$$\alpha\beta = -\alpha_z\beta_z. \tag{22}$$

Using the equations shown from (19) to (22), we obtained a dispersion diagram for the poles located using the ML expansion functions. Fig. 6 shows the normalized real component of k_x versus change in the dielectric thickness. The input parameters used to generate results shown in Fig. 6 are $f = 10$ GHz, $\varepsilon_r = 3.25$, and $\sigma \approx 9.42 \times 10^7$. Fig. 6(a) and (b) shows dispersion diagram for lossless and lossy cases, respectively.

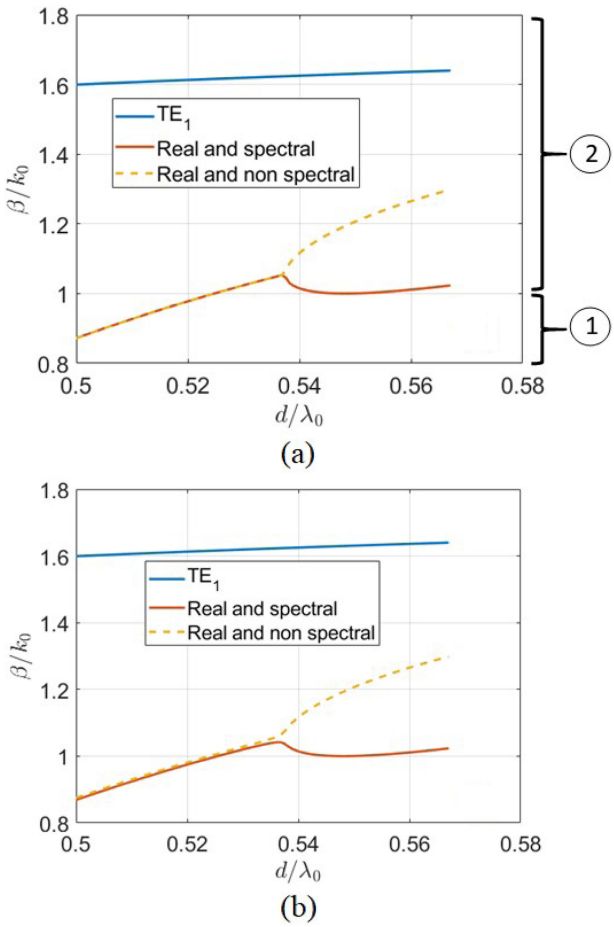

Fig. 6. Identifying real spectral and non-spectral SW modes obtained from the ML expansion functions.

The blue curve in Fig. 6(a) and (b) represents the dominant TE_1 mode. In Fig. 6, two regions (① and ②) are shown, where region ① represents LW modes and region ② represents SW modes. In Fig. 6, an LW emerges in region ①, i.e., for $\beta/k_0 < 1$. This curve continues above $\beta/k_0 = 1$, i.e., into region ②, thereby slowly transitioning into an SW mode. This mode, then, splits into two curves at around $d/\lambda = 0.5347$. The dashed yellow curve rises above representing a nonspectral behavior, i.e., an improper SW mode. The solid red line curves back, remains close to $\beta/k_0 = 1$ and rises back again, which is a behavior of spectral curve or of a proper SW mode. The nonspectral and spectral curves observed in Fig. 6(a) are similar to the curves shown in [37, Fig. 3]. In Fig. 6(b), same phenomena can be observed except that the two LW modes ($\beta/k_0 < 1$) never actually merges. One LW continues to be a real and nonspectral mode whereas the other one becomes a real and spectral mode. The attenuation constant (α) of LW modes with $\beta/k_0 < 1$ has two components, of which one satisfies the radiation condition at infinity and the other grows exponentially. These growing waves are represented as forward waves, which are shown as arrows pointing outwards and away from the interface in Fig. 5.

This article finally indicates that the second-order ML expansion function is capable of identifying all types of SW and LW poles. Same explanation can easily be extended to the case of D_{TM} using its corresponding first- or second-order ML expansion function depending on the value of $|l_r|$. If the electrical thickness of dielectric substrate further increases, the order of ML expansion function needs to be increased and by observing same steps, one can obtain and differentiate between various types of poles.

IV. Conclusion

A novel pole extraction method has been introduced and an in-depth numerical convergence study has been carried out using the ML expansion method. We have showed that the ML expansion method yields highest accuracy in predicting the initial pole location by using minimum number of expansion terms. This indicates that the ML expansion method is computationally inexpensive when searching for poles especially for ETS, whereas the performance of other methods became unpredictable or deteriorates with any change in the substrate configuration.

The NRMSE method further solidified the robustness of the ML expansion method for a range of dielectric permittivities and thicknesses. In addition, by using the Padé approximant, the initial pole location moved closer to the final pole location. The optimum Padé approximant was found to be $P_3^3(v)$ for the $m = 1$ and $m = 2$ expansion terms. The Padé approximant can be used specifically for very small tolerance factors effectively reducing the computational time used by traditional root-finding algorithms. Finally, in this article, it has been proved that the ML expansion method can locate both proper and improper SW poles, and has shown its effectiveness in isolating LW and SW modes, even for large electrical thicknesses.

References

[1] D. G. Duffy, *Green's Functions With Applications*. Boca Raton, FL, USA: Chapman & Hall/CRC, 2015.
[2] D. Pozar, "Considerations for millimeter wave printed antennas," *IEEE Trans. Antennas Propag.*, vol. AP-31, no. 5, pp. 740–747, Sep. 1983.
[3] M. Qiu, M. Simcoe, and G. V. Eleftheriades, "High-gain meanderless slot arrays on electrically thick substrates at millimeter-wave frequencies," *IEEE Trans. Microw. Theory Techn.*, vol. 50, no. 2, pp. 517–528, Aug. 2002.
[4] D. G. Duffy, "Response of a grounded dielectric slab to an impulse line source using leaky modes," *IEEE Trans. Antennas Propag.*, vol. 42, no. 3, pp. 340–346, Mar. 1994.
[5] A. M. Patel and A. Grbic, "A printed leaky-wave antenna based on a sinusoidally-modulated reactance surface," *IEEE Trans. Antennas Propag.*, vol. 59, no. 6, pp. 2087–2096, Jun. 2011.
[6] E. Chang, S. Long, and W. Richards, "An experimental investigation of electrically thick rectangular microstrip antennas," *IEEE Trans. Antennas Propag.*, vol. AP-34, no. 6, pp. 767–772, Jun. 1986.
[7] R. Garg and S. Long, "Resonant frequency of electrically thick rectangular microstrip antennas," *Electron. Lett.*, vol. 23, no. 21, pp. 1149–1151, Oct. 1987.
[8] D. Zheng and K. Michalski, "Analysis of coaxially fed microstrip antennas of arbitrary shape with thick substrates," *J. Electromagn. Waves Appl.*, vol. 5, no. 12, pp. 1303–1327, 1991.
[9] A. J. Parfitt, D. W. Griffin, and P. H. Cole, "On the modeling of metal strip antennas contiguous with the edge of electrically thick finite size dielectric substrates," *IEEE Trans. Antennas Propag.*, vol. 40, no. 2, pp. 134–140, Feb. 1992.
[10] A. J. Parfitt, D. W. Griffin, and P. H. Cole, "Mutual coupling between metal strip antennas on finite size, electrically thick dielectric substrates," *IEEE Trans. Antennas Propag.*, vol. 41, no. 1, pp. 108–115, Jan. 1993.

[11] G. M. Rebeiz, "Millimeter-wave and terahertz integrated circuit antennas," *Proc. IEEE*, vol. 80, no. 11, pp. 1748–1770, Nov. 1992.
[12] M. A. Hickey, M. Qiu, and G. V. Eleftheriades, "A reduced surface-wave twin arc-slot antenna for millimeter-wave applications," *IEEE Microw. Wireless Compon. Lett.*, vol. 11, no. 11, pp. 459–461, Nov. 2001.
[13] A. Shahvarpour, A. A. Melcon, and C. Caloz, "Radiation efficiency issues in planar antennas on electrically thick substrates and solutions," *IEEE Trans. Antennas Propag.*, vol. 61, no. 8, pp. 4013–4025, Aug. 2013.
[14] M. A. Marin, S. Barkeshli, and P. H. Pathak, "On the location of proper and improper surface wave poles for the grounded dielectric slab," *IEEE Trans. Antennas Propag.*, vol. 38, no. 4, pp. 570–573, Apr. 1990.
[15] C.-I. Hsu, R. F. Harrington, J. R. Mautz, and T. Sarkar, "On the location of leaky wave poles for a grounded dielectric slab," *IEEE Trans. Microw. Theory Techn.*, vol. 39, no. 2, pp. 346–349, Feb. 1991.
[16] F. Mesa and M. Horno, "Computation of proper and improper modes in multilayered bianisotropic waveguides," *IEEE Trans. Microw. Theory Techn.*, vol. 43, no. 1, pp. 233–235, Jan. 1995.
[17] M. J. Neve and R. Paknys, "A technique for approximating the location of surface-and leaky-wave poles for a lossy dielectric slab," *IEEE Trans. Antennas Propag.*, vol. 54, no. 1, pp. 115–120, Jan. 2006.
[18] A. Polimeridis, T. Yioultsis, and T. Tsiboukis, "An efficient pole extraction technique for the computation of green's functions in stratified media using a sine transformation," *IEEE Trans. Antennas Propag.*, vol. 55, no. 1, pp. 227–229, Jan. 2007.
[19] L. Tsang and B. Wu, "Electromagnetic fields of hertzian dipoles in layered media of moderate thickness including the effects of all modes," *IEEE Antennas Wireless Propag. Lett.*, vol. 6, pp. 316–319, Jul. 2007.
[20] S. Pan and J. Fan, "An efficient method to extract surface-wave poles of Green's functions near branch cut in lossy layered media," *IEEE Trans. Antennas Propag.*, vol. 63, no. 1, pp. 439–442, Jan. 2015.
[21] Z.-G. Qian and W. C. Chew, "Fast full-wave surface integral equation solver for multiscale structure modeling," *IEEE Trans. Antennas Propag.*, vol. 57, no. 11, pp. 3594–3601, Nov. 2009.
[22] W. C. Chew and L. J. Jiang, "Overview of large-scale computing: The past, the present, and the future," *Proc. IEEE*, vol. 101, no. 2, pp. 227–241, Feb. 2013.
[23] S. Karabasov, D. Nerukh, A. Hoekstra, B. Chopard, and P. V. Coveney, "Multiscale modelling: Approaches and challenges," *Philos. Trans. Roy. Soc.*, series A, vol. 372, no. 2021, Aug. 2014. [Online] Available: https://doi.org/10.1098/rsta.2013.0390
[24] E. Alanen, I. V. Lindell, and A. Hujanen, "Exact image method for field calculation in horizontally layered medium above a conducting ground plane," *IEE Proc. H-Microw., Antennas Propag.*, vol. 133, no. 4, pp. 297–304, Aug. 1986.
[25] K. C. Durbhakula, D. Chatterjee, and A. M. Hassan, "On the location of transverse electric surface wave poles for electrically thick substrates," in *Proc. IEEE Int. Symp. Antennas Propag. USNC/URSI Nat. Radio Sci. Meeting*, Atlanta, GA, USA, 2019, pp. 833–834.
[26] K. C. Durbhakula, D. Chatterjee, and A. M. Hassan, "Location of surface wave poles in sommerfeld type integrals: A Mittag-Leffler expansion approach," in *Proc. IEEE URSI Int. Symp. Electromagn. Theory*, San Diego, CA, USA, May 2019, pp. 1–4.
[27] S. Barkeshli, "Efficient approaches for evaluating the planar microstrip Green's function and its applications to the analysis of microstrip antennas," Ph.D. dissertation, The Ohio State Univ., Columbus, OH, USA, 1988.
[28] The Rogers Corporation. Accessed: Jun. 2019. [Online]. Available: https://www.rogerscorp.com/index.aspx
[29] M. Abramowitz and I. A. Stegun, *Handbook of Mathematical Functions: with Formulas, Graphs, and Mathematical Tables*. New York, NY, USA: Dover, 1965.
[30] C. M. Bender and S. A. Orszag, *Advanced Mathematical Methods for Scientists and Engineers I: Asymptotic Methods and Perturbation Theory*. New York, NY, USA: Springer, 1999.
[31] G. A. Baker Jr and P. Graves-Morris, *Padé Approximants*. Cambridge, U.K.: Cambridge Univ. Press, 1996.
[32] O. L. Ibryaeva and V. M. Adukov, "An algorithm for computing a padé approximant with minimal degree denominator," *J. Comput. Appl. Math.*, vol. 237, no. 1, pp. 529–541, Jan. 2013.
[33] T. K. Sheel, "Rational approximants generated by pade approximation and u-Transform," M.S. thesis, Dept. Math., Univ. Dhaka, Dhaka, Bangladesh, 1997.
[34] V. Galdi and I. M. Pinto, "A simple algorithm for accurate location of leaky-wave poles for grounded inhomogeneous dielectric slabs," *Microw. Opt. Technol. Lett.*, vol. 24, no. 2, pp. 135–140, Jan. 2000.
[35] L. B. Felsen and N. Marcuvitz, *Radiation and Scattering of Waves*. Piscataway, NJ, USA: IEEE Press, 1994.
[36] H. Shigesawa, M. Tsuji, and A. Oliner, "The nature of the spectral gap between bound and leaky solutions when dielectric loss is present in printed-circuit lines," *Radio Sci.*, vol. 28, no. 6, pp. 1235–1243, Nov. 1993.
[37] P. Lampariello, F. Frezza, and A. A. Oliner, "The transition region between bound-wave and leaky-wave ranges for a partially dielectric-loaded open guiding structure," *IEEE Trans. Microw. Theory Techn.*, vol. 38, no. 12, pp. 1831–1836, Dec. 1990.
[38] T. Tamir and A. A. Oliner, "Guided complex waves. Part 1: Fields at an interface," *Proc. Inst. Electr. Eng.*, vol. 110, no. 2, pp. 310–324, Feb. 1963.
[39] T. Tamir and A. A. Oliner, "Guided complex waves. Part 2: Relation to radiation patterns," *Proc. Inst. Electr. Eng.*, vol. 110, no. 2, pp. 325–334, Feb. 1963.
[40] S. S. Mangiafico, *Summary and Analysis of Extension Program Evaluation in R*. New Brunswick, NJ, USA: Rutgers Cooperative Extension, 2016.

Kalyan C. Durbhakula (Student Member, IEEE) received the B.Tech. degree in electronics and communication engineering from the MLR Institute of Technology, Hyderabad, India, in 2013 and the M.S. and Ph.D. degrees in electrical engineering from the University of Missouri-Kansas City (UMKC), Kansas City, MO, USA, in 2015 and 2019, respectively.

He is currently an Assistant Research Professor with the Missouri Institute of Defense and Energy, UMKC. His research interests include nanoelectromagnetics, computational electromagnetics, multilayered Green's functions, characteristic mode analysis, experimental microwave, and EMI/EMC analysis.

Dr. Kalyan Durbhakula received the UMKC's School of Graduate Studies Research Grant Award in 2016.

Deb Chatterjee (Senior Member, IEEE) received the B.Tech. degree in electrical engineering from Jadavpur University, Kolkata, India, in 1982, the M.Tech. degree from Indian Institute of Technology Kharagpur, Kharagpur, India, in 1984, the M.A.Sc. degree from Concordia University, Montréal, QC, Canada, in 1992, and the Ph.D. degree from the University of Kansas, Lawrence, KS, USA, in 1998.

He was an ONR-ASEE Summer Faculty Fellow with the Naval Research Laboratory, Washington, DC, USA, from 2009 to 2014. He is currently an Associate Professor with the Department of Computer Science and Electrical Engineering, University of Missouri at Kansas City, Kansas City, MO, USA. His current research interests include asymptotic techniques, multilayer Green's functions, characteristic mode theory and applications, electronic packaging, and microwave imaging.

Ahmed M. Hassan (Senior Member, IEEE) received the B.Sc. degree (with highest hons.) and the M.Sc. degree from Cairo University, Giza, Egypt, in 2004 and 2006, respectively, both in electronics and communications engineering. He received the Ph.D. degree in electrical engineering from the University of Arkansas, Fayetteville, AR, USA, in 2010.

From 2011 to 2012, he was a Postdoctoral Researcher with the Department of Electrical Engineering, University of Arkansas. From 2012 to 2015, he was a Postdoctoral Researcher with the National Institute of Standards and Technology, Gaithersburg, MD, USA. He is currently an Assistant Professor with the Department of Computer Science and Electrical Engineering, University of Missouri-Kansas City. His current research interests include nanoelectromagnetics, bioelectromagnetics, nondestructive evaluation, experimental microwave, and terahertz imaging.

Dr. Hassan received the 2017 University of Missouri-Kansas City CSEE Excellence in Teaching Award, the 2014 Outstanding Poster Award in the 21st Annual NIST Sigma Xi Postdoctoral Poster Presentation, and the 2007 Doctoral Academy Fellowship at the University of Arkansas.